Pacific Northwest
NATIONAL LABORATORY

PNNL-36668

Achieving high-ZT in Te/Se-based thermoelectric materials via volume-constrained shear-induced plastic deformation

September 2024

Tianhao Wang (PI)
Zexi Lu (Co-PI)
Tingkun Liu
Hyoju Park
David Garcia
Dongsheng Li
Scott A. Whalen (Mentor)

U.S. DEPARTMENT OF ENERGY

Prepared for the U.S. Department of Energy
under Contract DE-AC05-76RL01830

DISCLAIMER

PACIFIC NORTHWEST NATIONAL LABORATORY
operated by
BATTELLE
for the
UNITED STATES DEPARTMENT OF ENERGY
under Contract DE-AC05-76RL01830

Printed in the United States of America

Available to DOE and DOE contractors from
the Office of Scientific and Technical Information,
P.O. Box 62, Oak Ridge, TN 37831-0062
www.osti.gov
ph: (865) 576-8401
fox: (865) 576-5728
email: reports@osti.gov

Available to the public from the National Technical Information Service
5301 Shawnee Rd., Alexandria, VA 22312
ph: (800) 553-NTIS (6847)
or (703) 605-6000
email: info@ntis.gov
Online ordering: http://www.ntis.gov

PNNL-36668

Achieving high-ZT in Te/Se-based thermoelectric materials via volume-constrained shear-induced plastic deformation

September 2024

Tianhao Wang (PI)
Zexi Lu (Co-PI)
Tingkun Liu
Hyoju Park
David Garcia
Dongsheng Li
Scott A. Whalen (Mentor)

Prepared for
the U.S. Department of Energy
under Contract DE-AC05-76RL01830

Pacific Northwest National Laboratory
Richland, Washington 99354

Abstract

This study investigated the correlation between severe plastic deformation and microstructural evolution, along with the corresponding response in the thermoelectric performance. Specifically, severe plastic deformation introduced into intrinsically brittle thermoelectric materials like $Bi_2Te_{3-x}Se_x$ leads to microstructural changes ranging from nano- to micro- scales, including phase transformation, phase segregation, and stacking faults. The resultant residual strain and lattice defects in the $Bi_2Te_{3-x}Se_x$ materials led to engineering of electronic bands, which increases the effective mass of electrons while controlling their concentration, thereby enhancing the power factor.

Summary

This project aims to fabricate high-efficiency $Bi_2Te_{3-x}Se_x$-based room-temperature thermoelectric materials, using a combination of theoretical predictions based on atomistic and numerical simulations, and a novel technique exclusive to PNNL: the volume-constrained shear-induced plastic deformation method.

Acknowledgments

This research was supported by the Energy Mission Seed Investment, under the Laboratory Directed Research and Development (LDRD) Program at Pacific Northwest National Laboratory (PNNL). PNNL is a multi-program national laboratory operated for the U.S. Department of Energy (DOE) by Battelle Memorial Institute under Contract No. DE-AC05-76RL01830.

Acronyms and Abbreviations

- Scanning electron microscopy, SEM
- Energy-dispersive spectroscopy, EDS
- Transmission Electron Microscopy, TEM
- High resolution Transmission Electron Microscopy, HR-TEM
- X-ray diffraction, XRD
- Electron backscatter diffraction, EBSD
- Density functional theory, DFT
- Boltzmann transport equations, BTE

Contents

Figures

Tables

1.0 Introduction

Thermoelectric (TE) materials and devices provide direct conversion between heat and electricity based on the Seebeck effect. Poised as sustainable and ecofriendly energy resources, they provide promising alternatives to the conventional ones in helping meet the challenges of ever-growing global energy consumption (Su et al. 2022; Shi, Zou, and Chen 2020). However, their applications have since been limited by their energy conversion efficiency, measured by the dimensionless figure-of-merit, *ZT*:

$$ZT = \frac{S^2\sigma}{k}T = \frac{S^2\sigma}{k_e + k_p}T$$

where *S* is the Seebeck coefficient, σ is the electrical conductivity, *k* is the thermal conductivity, *T* is the absolute temperature, k_e is the electronic thermal conductivity, and k_p is the phonon or lattice thermal conductivity. Over the years, efforts have been made to enhance the performance (energy conversion efficiency), which implies an increase in *ZT* of TE devices mainly by either discovering new candidate materials, or tunning the micro/nano-structure of the devices for high power factor $S^2\sigma$ and low thermal conductivity (Shi, Zou, and Chen 2020; Li et al. 2021). However, both have only achieved limited progress especially when considering scaling-up for practical applications. Conventional TE materials are usually semiconductors (such as Bi_2Te_3, Ag_2Se, etc.) or high-entropy complex materials (such as $Yb_{14}MnSb_{11}$ etc.) (Snyder and Toberer 2008). The brittleness, a common feature shared by these materials, presents a significant challenge in their further processing for potentially enhanced TE properties; thus, they are often used directly after sintering without post-processing. As a result, the as-synthesized crystalline structures give rise to another limitation of the coupling between electrical and thermal conductivity (Wiedemann–Franz law) where the power factor cannot be enhanced without increasing the thermal conductivity. As such, a significant knowledge gap exists in the fundamental understanding of how to enhance *ZT* through further processing beyond syntheses in the intrinsically-brittle conventional TE materials, especially the microstructural effects on electron-phonon transport at atomic and sub-atomic levels, while the corresponding technical approach is also missing. Filling these gaps will certainly enable us to greatly enlarge the scope of candidate TE materials and raise the limit of their energy conversion efficiency for practical applications.

With the novel volume-constrained shear-induced plastic deformation, developed by and exclusive to PNNL, we are now able to introduce plastic deformation to the intrinsically-brittle TE materials, which cannot be achieved before or by other research institutions. Our preliminary studies have demonstrated that structural changes, from nano- to micro- scales including phase transformation and amorphization, can occur in brittle materials after the plastic deformation; therefore, we propose two hypotheses: the residual strain and micro/nano-structures in Te/Se-based TE materials, generated by volume-constrained shear-induced plastic deformation, can further lead to 1) engineering of electronic bands that can increase the effective mass of electrons while controlling their concentration, resulting in an enhanced power factor (as similar effects have been observed in previous studies (Hong et al. 2008; Milovanović et al. 2020)), and 2) tunning of electron-phonon transport, achieved by micro/nano-structures caused by amorphization and phase transformation that affect the mobility of quasi-particles of certain wavelengths (as is in previous studies (Chakraborty, Cao, and Wang 2017; He et al. 2020)).

2.0 Methodology

The n-type Bi_2Te_3 samples were purchased from Hi-Z Technology Inc. The as-received discs are 25.4 mm in diameter and 1.8 mm in thickness. Mass spectrometry measurement reveals that the sample is doped with Se, with the concentration ratio n_{Te}:n_{Se} of approximately 8.3:1. The grain sizes and orientations and crystallographic structures were characterized by scanning and transmission electron microscopy (SEM and TEM), energy-dispersive spectroscopy (EDS), and electron backscatter diffraction (EBSD). The thermoelectric properties at micro- to nano- scales were calibrated by atomistic simulations. The detailed approaches are outlined below:

2.1 Volume-constrained plastic deformation of $Bi_2Te_{3-x}Se_x$ discs

During the process, a rotating tool applies pressure and torsion to the feedstock disc, generating frictional heat and severe plastic deformation. A key benefit of this method is the combination of shear and pressing. Dynamic recrystallization occurs within the shearing zone, allowing for the attainment of a preferred texture. As shown in Figure 1, the rotating tool is installed in a Transformation Technologies, Inc. (TTI) friction stir welding (FSW) gantry machine, which controls the tool's rotational speed and axial force. These parameters can be adjusted to achieve the desired temperature, pressure, and torque conditions. An argon cover gas was used to minimize oxidation of the Bi_2Te_3 during processing. As shown in Figure 2, the process temperature for Runs 1-3 were monitored and plotted. The peak temperature reached approximately 400°C. As the process time increased, the temperature fluctuated between 300°C and 400°C, as shown in Run 3.

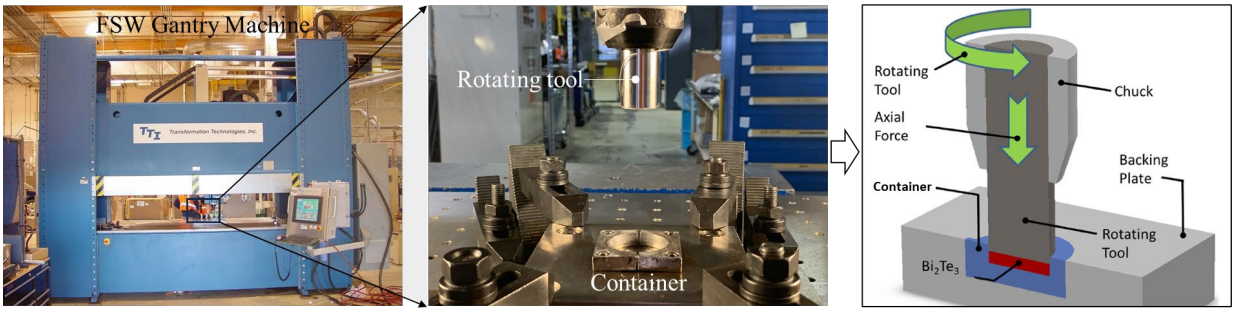

Figure 1. Friction stir welding (FSW) gantry machine, process setup, and schematic of the volume-constrained plastic deformation process.

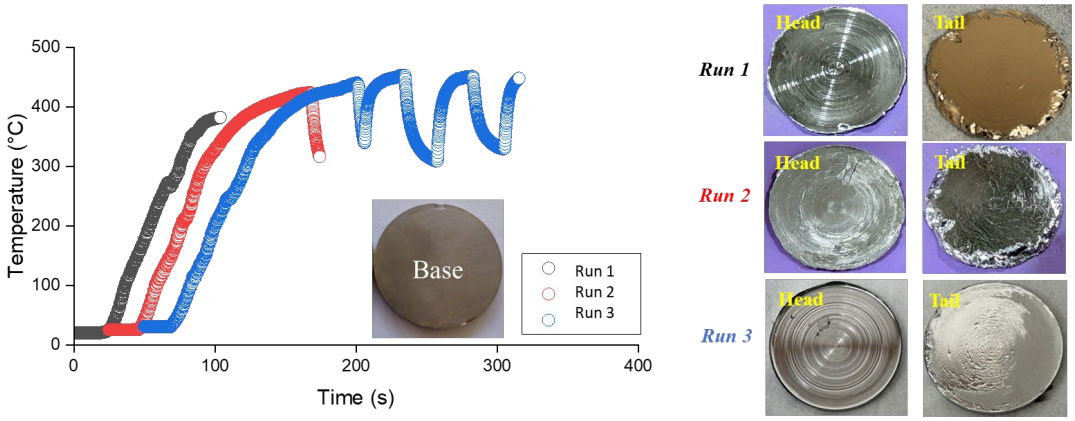

Figure 2. Processing temperatures for Run 1, Run 2, and Run 3. Pictures of processed discs.

2.2 Micro- and nano-scale characterization of crystal structures in processed $Bi_2Te_{3-x}Se_x$ samples

X-ray diffraction (XRD) measurements were conducted using a Rigaku D/Max Rapid II microdiffraction system. X-rays were generated by a MicroMax 007HF generator from a rotating Cr target (λ =2.2910 Å) and focused through a 10-μm-diameter collimator directly onto a region of interest identified using an integral video microscope. A two-dimensional image plate was used to collect diffraction data. XRD was collected using a 300-μm-diameter collimator directly from a region of interest with oscillating incident angles from 25° to 35°. The SEM-EDS and EBSD were conducted using a Thermo Fisher Scientific Helios 5 Hydra Scanning Electron Microscope implemented with Oxford Ultim Max EDS detector and Symmetry EBSD detector. The site-specific lift-out for the STEM analysis was prepared using an FEI Quanta 3D Focused Ion Beam SEM. Most of High-resolution STEM imaging was conducted on a Cs-corrected JEOL GrandARM at 300 kV. Atomic STEM-EDS maps were acquired using Themis, Thermo Fisher Scientific Inc. at 300 kV.

2.3 Atomistic simulations

We chose DFT as the theoretical approach as it is a first-principles computational chemistry method that allows us to investigate the electronic properties of the alloys from an atomic-scale, which is necessary as this information has been lacking in previous literatures. All simulations were performed using the Vienna Ab Initio Simulation Package (VASP) (Kresse and Hafner 1993) (Kresse and Furthmuller 1996). The core electrons were represented using projector-augmented-wave pseudopotentials (Blochl 1994; Kresse and Joubert 1999), and the generalized gradient approximation Perdew–Burke–Ernzerhof exchange-correlation functional was used (Perdew, Burke, and Ernzerhof 1996). A universal cutoff of 400 eV was used for all calculations, and the convergence threshold was set to 10^{-5} eV. The DFT-D3 dispersion correction for van der Waals interactions by Grimme et. al. was applied in all simulations (Grimme et al. 2016). The electronic structures were then passed on to Boltzmann transport equations to solve for the Seebeck coefficients, which was performed by the BoltzTrap2 package (Madsen, Carrete, and Verstraete 2018). The ab initio thermodynamic (AIT) calculations were performed using VASP and Phonopy (Togo et al. 2023), and the thermal conductivity was calculated using Phonopy and Phonon3py (Togo et al. 2023).

3.0 Results and discussion

3.1 Characterization of the as-received $Bi_2Te_{3-x}Se_x$ samples

We performed SEM and EDS measurements of the as received, or base $Bi_2Te_{2.67}Se_{0.33}$ samples. Figure. 3 shows the distribution of all three elements, and their atomic concentration is listed in Table. 1. The atomic ratio of n_{Te}:n_{Se} measured by EDS is 7.6:1, lower than that measured by mass spectroscopy (8.3:1). We attribute this difference to the localization effect, as EDS only analyzes a micro-sized region, while mass spectroscopy encompasses the entire sample on the order of millimeters. As such, we approximated the ratio as 8:1 for facile analyses, so that the chemical formula of the doped sample effectively becomes $Bi_2Te_{2.67}Se_{0.33}$.

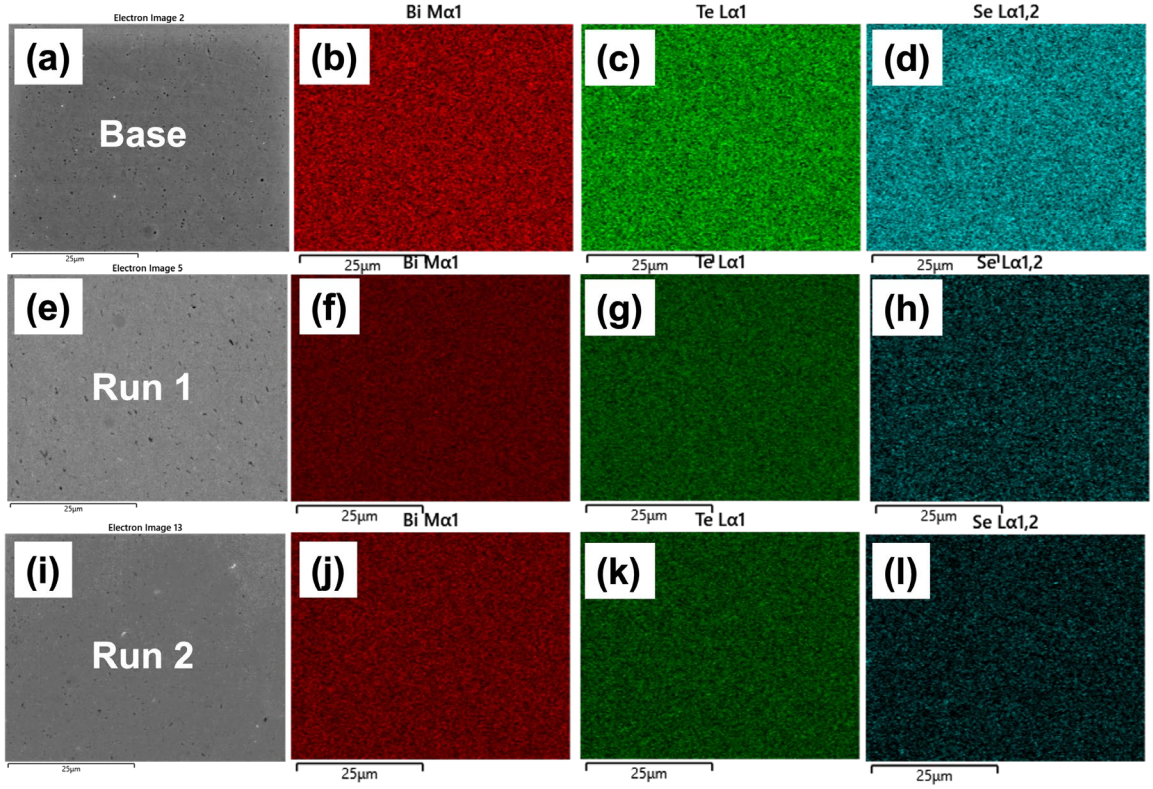

Figure 3. SEM and EDS images of (a-d) the as-received, or base, (e-h) Run 1, and (i-l) Run 2 $Bi_2Te_{2.67}Se_{0.33}$ samples, showing the distribution of (b, f, j) Bi, (c, g, k) Te, and (d, h, l) Se atoms.

Table 1. Atomic concentrations of the base, Run 1, and Run 2 samples measured by EDS

	Elemental concentration			
Sample	Bi	Te	Se	n_{Te}:n_{Se}
Base	40.10	52.96	6.94	7.6:1
Run 1	40.10	52.96	6.94	7.6:1
Run 2	40.10	52.96	6.94	7.6:1

XRD measurements (Figure. 4) reveal that all crystallites in the sample have the rhombohedral structure with the R-3m space group, which is the most thermodynamically stable structure of Bi_2Te_3. This is corroborated by TEM observation (Figure. 5) of the detailed lattice structure, where the characteristic quintuple atomic layers held together by van der Waals forces are clearly seen in each grain.

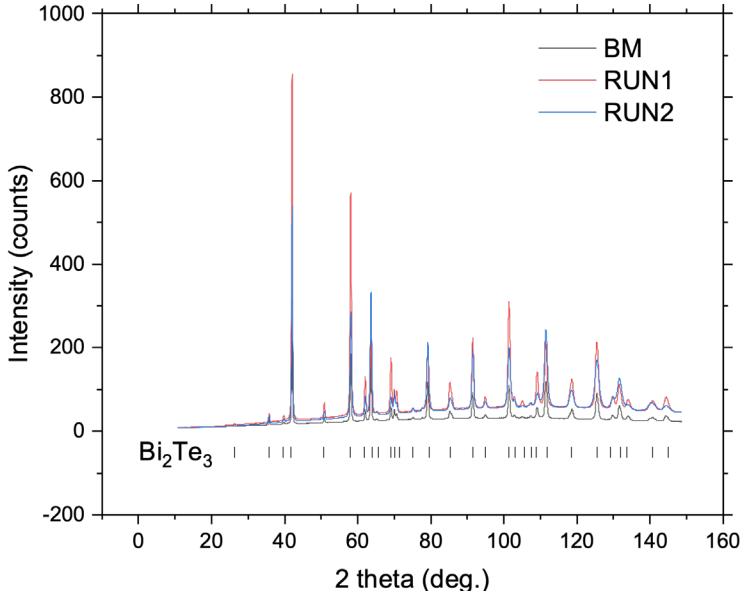

Figure 4. XRD measurement identifies all samples as the rhombohedral Bi_2Te_3.

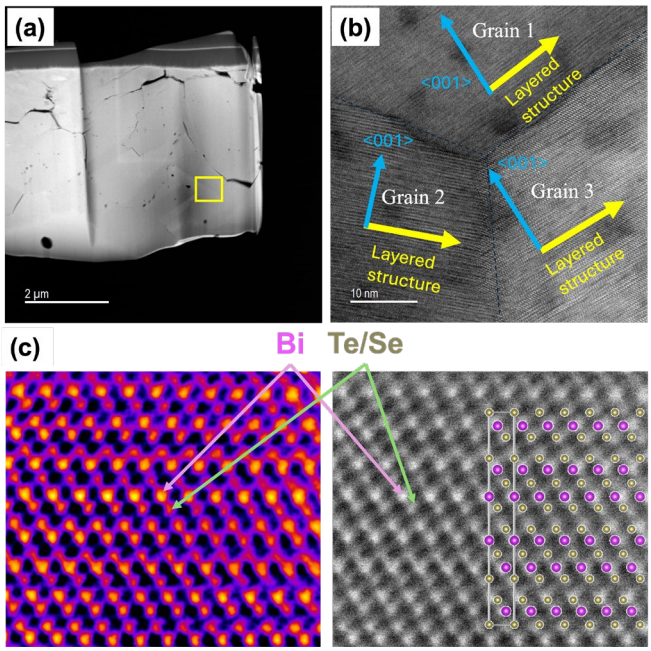

Figure 5. (a) SEM and (b-c) TEM characterization of the base $Bi_2Te_{2.67}Se_{0.33}$ samples. The layered structure can be clearly observed within one single-crystal grain. An overlay of the lattice structure of Bi_2Te_3 is shown to visually guide the positions of Bi and Te/Se atoms.

3.2 The effect of plastic deformation on the crystalline structures and thermoelectric properties of $Bi_2Te_{2.67}Se_{0.33}$

We first characterized the texture change of the samples using EBSD. As shown in Figure 6, significant texture change in the processed top region has been observed. Nearly 100% of the grains are aligned along their <001> crystallographic orientations, while the change in grain sizes is negligible. TEM observations (Figure. 7) of the crystallites reveal that the rhombohedral lattice structure remains the same after processing. Here we estimated the *ZT* values based on our own atomistic simulations of pure Bi_2Te_3. A 1×1×1 Bi_2Te_3 conventional unit cell was optimized using VASP based on a 4×4×1 k-mesh, yielding lattice constants of a=b=4.41 Å and c=32.25 Å. The electronic structures were then evaluated based on an 8×8×2 k-mesh, and the calculated band structures were then passed to BoltzTrap2 to evaluate the Seebeck coefficient and electrical conductivity based on Boltzmann transport equations. The optimized structure was then passed to Phonopy which calculates the phonon dispersion based on frozen phonon methods, and Phono3py which calculates the thermal conductivity based on the phonon dispersion and Boltzmann transport equations. According to our own calculations, the figures of merit along and normal to the basal plane {001} are different by ~30%: $ZT_{\parallel}/ZT_{\perp}\approx1.3$. As such, assuming the lattice structures of $Bi_2Te_{2.67}Se_{0.33}$ remain the same within each grain, then the enhancement in overall *ZT* resulting from texture alone ~15% along the <100> directions.

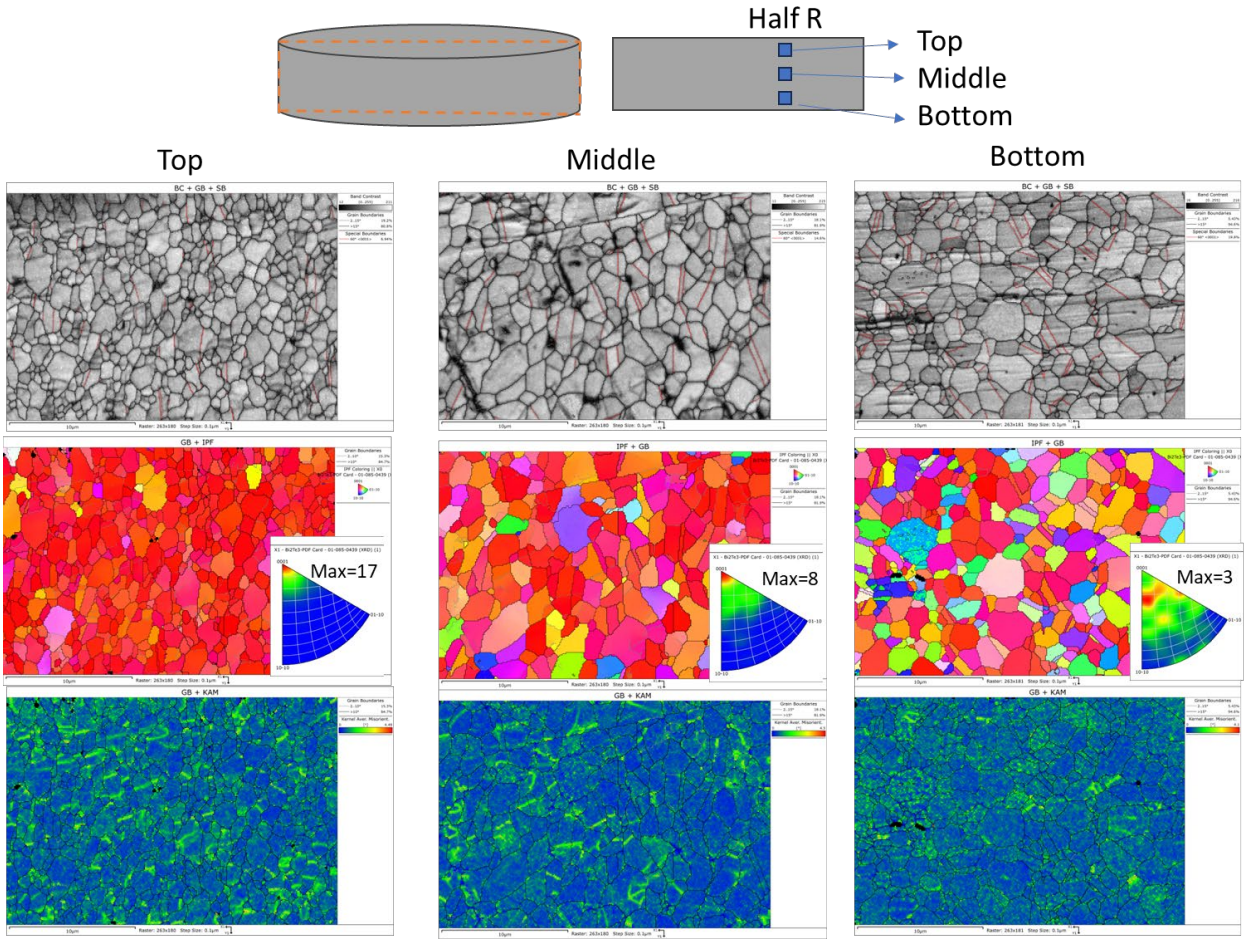

Figure 6. EBSD analysis on the different locations of Run 1.

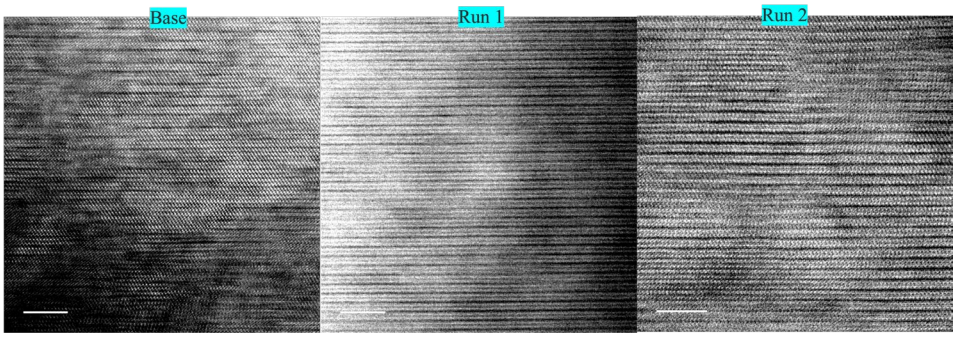

Figure 7. Comparison of TEM observations of the base and processed samples reveals that the rhombohedral lattice structure remains.

Further characterization of the elemental distribution using atomic-resolution EDS (Figure. 8) shows that Se atoms substitute Te atoms homogeneously while Bi atoms stay in their intrinsic positions. This is corroborated by our AIT calculations, which shows that in $Bi_2Te_{2.67}Se_{0.33}$ a random distribution of Se atoms is thermodynamically preferred. We compare the structures of $Bi_2Te_{2.67}Se_{0.33}$ with different Se atom positioning (Figure. 9). In a conventional rhombohedral unit cell of Bi_2Te_3, there are six unique Bi atoms and nine unique Te atoms (six equivalents forming the van der Waals gaps, and the other three equivalents between the Bi atoms). We approximate the different $Bi_2Te_{2.67}Se_{0.33}$ structures using two cases: by replacing the Te atom 1) in the van der Waals gap, or 2) between the Bi atoms with a Se atom. Both resulting structures represent an effective bulk $Bi_2Te_{2.67}Se_{0.33}$ where entire planes of Te atoms are replaced by Se, which we assume present the extreme cases of Se substitution and signifies its effect on thermodynamic stabilities. As such, we optimized the two structures using VASP, which were then passed to Phonopy to calculate the zero-point energies and temperature-dependent Gibbs free energy. The Gibbs free energy of formation was then evaluated by subtracting the free energy of the most stable reference forms, i.e. solid-phase Bi, Te, and Se. The results show that the two structures have almost identical Gibbs free energies of formation (difference < 0.1%), indicating that the Se atoms do not have specific energetically preferable positions and likely substitute Te atoms randomly. As such, we postulate that our estimated simulations of the sample using homogeneous Bi_2Te_3 is reasonable.

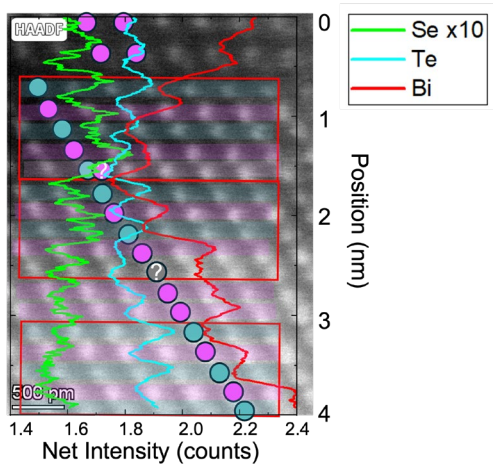

Figure 8. Atomic-resolution EDS reveals the detailed elemental distribution at each lattice point. Se atoms substitute Te atoms homogeneously while Bi atoms stay in their intrinsic positions.

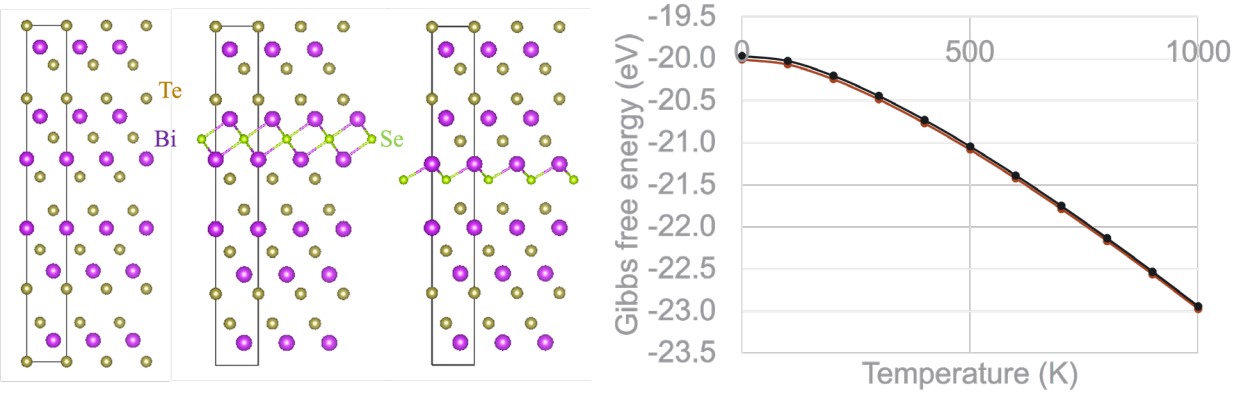

Figure 9. AIT calculations of Bi2Te2.67Se0.33 of different structures reveal that different positionings of Se atoms are almost thermodynamically equivalent, as the Gibbs free energies of formation of different structures are almost identical (difference < 0.1%).

A further characterization using SEM and EDS across grain boundaries, however, did find inhomogeneity among the elements. As shown in Figure. 10, there is apparent Se segregation at the grain boundaries, seemingly substituting Bi atoms. Further TEM characterizations in follow-up studies are needed to identify the detailed atomic structures.

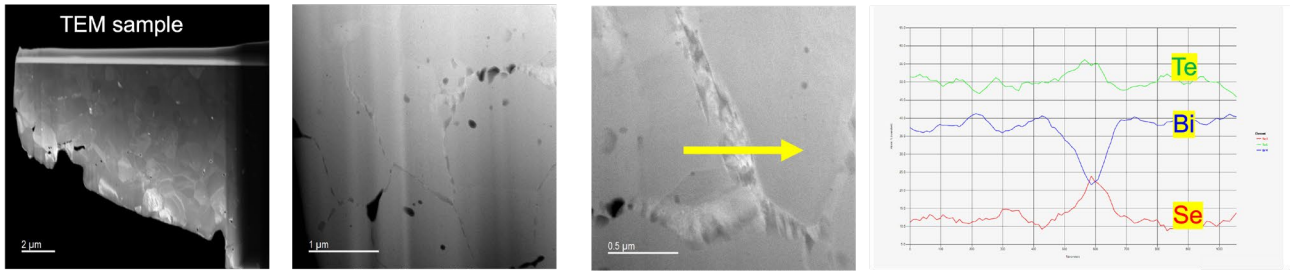

Figure 10. TEM and EDS review Se segregation across grain boundaries in the processed samples.

A notable feature in the processed $Bi_2Te_{2.67}Se_{0.33}$ samples is the strain field, induced by dislocations and stacking faults as shown in Figure. 11. To analyze their effect on the thermoelectric properties, we conducted DFT simulations to estimate the Seebeck coefficient S of the sample. The simulation box consists of 1×1×1 Bi_2Te_3 conventional rhombohedral unit cell using based on the same footings as aforementioned simulations. For the strain-free structure, the Boltzmann transport equations calculation predicts Seebeck coefficients of $S_{||}$=53.9 μV and $S_{\perp}$=40.2 μV.

To simulate the effect of strains, we stretch the optimized simulation cell along the <100> direction by ~3%, and then fixed the cell while relaxing the internal coordinates. The Seebeck coefficients of the resultant structure are $S_{||}$=70.2 μV and $S_{\perp}$=63.3 μV. Compared with the strain-free structure, a 3% tensile strain can lead to a stunning ~60% increase in the Seebeck coefficient along both directions. Further analyses based on the electronic band structures reveal that this originates from the “band-flattening” effect near the Fermi surface. This means that with the presence of tensile strains, the gradient of the electronic bands near the Fermi level becomes smaller and consequently the electrons have a larger effective mass, leading to an increase in Seebeck coefficient. This is consistent with our first hypothesis, that volume-

constrained shear-induced plastic deformation can lead to engineering of electronic bands which can increase the effective mass of electrons while controlling their concentration, resulting in an enhanced power factor. Similarly, for a 3% compression, the Seebeck coefficients are $S_{||}$=39.2 μV and $S_{\perp}$=28.9 μV, which are approximately 73% of their strain-free counterparts, respectively.

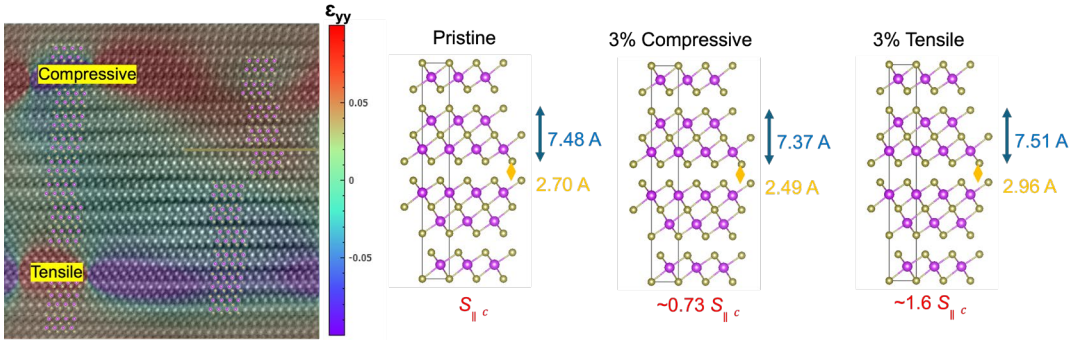

Figure 11. TEM measured strain field and the corresponding atomic structures used in DFT simulations.

4.0 Conclusion

This study investigated achieving high-ZT in Te/Se-based thermoelectric materials via volume-constrained, shear-induced plastic deformation. The main conclusions are as follows:

- The method of volume-constrained, shear-induced plastic deformation effectively aligns the grain texture along the shear-processing direction within the processed zone.
- In the base sample, Se substitutes Te atoms randomly, as revealed by atomic-resolution EDS and supported by AIT simulations. Se segregation across grain boundaries occurs in the processed zone, confirmed by TEM.
- The strain field significantly affects the thermoelectric properties. A 3% tensile strain can increase the Seebeck coefficient by approximately 60%, while a 3% compression can reduce it by about 27%, as confirmed by DFT simulations.

5.0 References

Blochl, P. E. 1994. "Projector Augmented-Wave Method." *Physical Review B* 50 (24): 17953-17979. https://doi.org/DOI 10.1103/PhysRevB.50.17953. <Go to ISI>://WOS:A1994QB02200016.

Chakraborty, Pranay, Lei Cao, and Yan Wang. 2017. "Ultralow Lattice Thermal Conductivity of the Random Multilayer Structure with Lattice Imperfections." *Scientific Reports* 7 (1): 8134. https://doi.org/10.1038/s41598-017-08359-2. https://doi.org/10.1038/s41598-017-08359-2.

Grimme, Stefan, Andreas Hansen, Jan Gerit Brandenburg, and Christoph Bannwarth. 2016. "Dispersion-Corrected Mean-Field Electronic Structure Methods." *Chemical Reviews* 116 (9): 5105-5154. https://doi.org/10.1021/acs.chemrev.5b00533. https://doi.org/10.1021/acs.chemrev.5b00533.

He, Shiyang, Yongbo Li, Lu Liu, Ying Jiang, Jingjing Feng, Wei Zhu, Jiye Zhang, Zirui Dong, Yuan Deng, Jun Luo, Wenqing Zhang, and Gang Chen. 2020. "Semiconductor glass with superior flexibility and high room temperature thermoelectric performance." *Science Advances* 6 (15): eaaz8423. https://doi.org/10.1126/sciadv.aaz8423. https://doi.org/10.1126/sciadv.aaz8423.

Hong, Ki-Ha, Jongseob Kim, Sung-Hoon Lee, and Jai Kwang Shin. 2008. "Strain-Driven Electronic Band Structure Modulation of Si Nanowires." *Nano Letters* 8 (5): 1335-1340. https://doi.org/10.1021/nl0734140. https://doi.org/10.1021/nl0734140.

Kresse, G., and J. Furthmuller. 1996. "Efficiency of ab-initio total energy calculations for metals and semiconductors using a plane-wave basis set." *Computational Materials Science* 6 (1): 15-50. https://doi.org/Doi 10.1016/0927-0256(96)00008-0. <Go to ISI>://WOS:A1996VF38900003.

Kresse, G., and J. Hafner. 1993. "Ab initio molecular dynamics for liquid metals." *Physical Review B* 47 (1): 558-561. https://doi.org/10.1103/PhysRevB.47.558. https://link.aps.org/doi/10.1103/PhysRevB.47.558.

Kresse, G., and D. Joubert. 1999. "From ultrasoft pseudopotentials to the projector augmented-wave method." *Physical Review B* 59 (3): 1758-1775. https://doi.org/DOI 10.1103/PhysRevB.59.1758. <Go to ISI>://WOS:000078291000045.

Li, Qingyi, Zichen Wei, Quanying Ma, Zhili Li, and Jun Luo. 2021. "Optimizing Room-Temperature Thermoelectric Performance of n-Type Bi2Te2.7Se0.3." *ACS Omega* 6 (49): 33883-33888. https://doi.org/10.1021/acsomega.1c05160. https://doi.org/10.1021/acsomega.1c05160.

Madsen, Georg K. H., Jesús Carrete, and Matthieu J. Verstraete. 2018. "BoltzTraP2, a program for interpolating band structures and calculating semi-classical transport coefficients." *Computer Physics Communications* 231: 140-145. https://doi.org/https://doi.org/10.1016/j.cpc.2018.05.010. https://www.sciencedirect.com/science/article/pii/S0010465518301632.

Milovanović, S. P., M. Anđelković, L. Covaci, and F. M. Peeters. 2020. "Band flattening in buckled monolayer graphene." *Physical Review B* 102 (24): 245427. https://doi.org/10.1103/PhysRevB.102.245427. https://link.aps.org/doi/10.1103/PhysRevB.102.245427.

Perdew, J. P., K. Burke, and M. Ernzerhof. 1996. "Generalized gradient approximation made simple." *Physical Review Letters* 77 (18): 3865-3868. https://doi.org/DOI 10.1103/PhysRevLett.77.3865. <Go to ISI>://WOS:A1996VP22500044.

Shi, Xiao-Lei, Jin Zou, and Zhi-Gang Chen. 2020. "Advanced Thermoelectric Design: From Materials and Structures to Devices." *Chemical Reviews* 120 (15): 7399-7515.

https://doi.org/10.1021/acs.chemrev.0c00026.
https://doi.org/10.1021/acs.chemrev.0c00026.

Snyder, G. Jeffrey, and Eric S. Toberer. 2008. "Complex thermoelectric materials." *Nature Materials* 7 (2): 105-114. https://doi.org/10.1038/nmat2090.
https://doi.org/10.1038/nmat2090.

Su, Lizhong, Dongyang Wang, Sining Wang, Bingchao Qin, Yuping Wang, Yongxin Qin, Yang Jin, Cheng Chang, and Li-Dong Zhao. 2022. "High thermoelectric performance realized through manipulating layered phonon-electron decoupling." *Science* 375 (6587): 1385-1389. https://doi.org/10.1126/science.abn8997. https://doi.org/10.1126/science.abn8997.

Togo, Atsushi, Laurent Chaput, Terumasa Tadano, and Isao Tanaka. 2023. "Implementation strategies in phonopy and phono3py." *Journal of Physics: Condensed Matter* 35 (35): 353001. https://doi.org/10.1088/1361-648X/acd831. https://dx.doi.org/10.1088/1361-648X/acd831.

Pacific Northwest National Laboratory

902 Battelle Boulevard
P.O. Box 999
Richland, WA 99354

1-888-375-PNNL (7665)

www.pnnl.gov